Some comments on the effect of uranium zonation on fission track dating by LA-ICP-MS

Nathan Cogné, Kerry Gallagher

1 **Some comments on the effect of uranium zonation on fission track dating by**

2 **LA-ICP-MS**

3

4 Nathan Cogné*[1] and Kerry Gallagher[1]

5 [1]Univ Rennes, CNRS, Géosciences Rennes, UMR 6118, 35000 Rennes, France

6 *corresponding author: nathan.cogne@univ-rennes1.fr

7

8 <u>Abstract</u>

9   The use of LA-ICP-MS for uranium determination in the fission track dating

10 technique is becoming increasingly popular because of several advantages over the

11 classical external detector method and a variety of analytical and statistical protocols

12 have been developed. However, two important issues remain unresolved in the

13 context of the LA-ICP-MS approach (i) how to best deal with low track density (ρ_s)

14 samples, and (ii) does a correlation between age and uranium content (or eU) reflect

15 an annealing dependence or not? To assess the impact of the analytical

16 methodology on these issues, we compare the multi-spot and more classical single

17 spot methods on samples of known ages, variably zoned and / or with low track

18 densities. To make the comparison we use an approach, implemented in a Python

19 script, that randomly samples our multi-spot ICP-MS data to choose a single U

20 measurement per grain, simulating the single spot approach. We then calculate the

21 central age, $p(\chi^2)$ and dispersion of the simulated single spot analysis and repeat this

22 2000 times. Our results show that the multi-spot approach is robust for low ρ_s and

23 zoned samples, yielding both accurate and precise results without over-dispersion.

24 Additionally, our random sampling approach shows that a single spot measurement

25 can induce an overdispersion coupled to a relationship between single grain age and

26 U content. This is at least partly attributable to zonation that creates a mismatch

27 between the U in the counted area and the spot-measured U. Therefore, we

28 recommend that if over-dispersion is observed for basement samples, when one

29 typically expects a single age population, then multiple spot analysis should be

30 carried out to assess if the excess dispersion is linked to undetected zoning and / or

31 laser spot misplacement rather than to U dependent annealing behaviour.

32

33 Keywords: Fission track dating; LA-ICP-MS; single grain age dispersion; Uranium

34 zonation

35

36 <u>1- Introduction</u>

37 Fission track dating is a thermochronological method based on the creation of

38 defects (tracks) during the spontaneous fission of ^{238}U. These latent tracks can be

39 revealed with an appropriate chemical etching protocol and then observed under an

40 optical microscope (Price and Walker, 1962). As part of the analytical procedure, it is

41 necessary to estimate the uranium (U) content of the mineral being dated. Towards

42 the end of the 20th century a consensus on the ζ (zeta) calibration approach and the

43 external detector method (EDM) was reached (Hurford and Green, 1983, Hurford,

44 1990). The EDM protocol consists of irradiating the targeted mineral to induce fission

45 of ^{235}U providing an indirect measure of ^{238}U when calibrated against a dosimeter or

46 standard glass of known U concentration. The mineral being dated is etched prior to

47 irradiation and then placed in intimate contact with a low-U detector, usually a

48 muscovite sheet. After irradiation the induced tracks are then revealed by etching the

49 detector. The ζ approach regroups the thermal flux of the neutron irradiation and the

50 fission decay constant, historically often considered to be not well defined, in a single

2

51 calibration factor, ζ (see Hurford and Green, 1983 for more details). This factor is

52 estimated by analyzing samples of known ages and recasting the age equation in

53 terms of ζ as an unknown. Despite the advantages of this coupled approach, the

54 EDM suffers from some setbacks including (i) the need for three different counts of

55 tracks: in the mineral, the detector and the dosimeter and (ii) the manipulation of

56 hazardous hydrofluoric acid to etch the muscovite detector (iii) increasingly difficult

57 access to low energy neutron irradiation to induce fission tracks in the detector.

58   Therefore, during the early 2000's researchers explored the use of LA-ICP-MS

59 to determine U concentration of the mineral to be dated. Hasebe et al. (2004)

60 demonstrated the feasibility of this technique. During the past decade several

61 protocols have been developed for FT dating, mainly on the calcium-phosphate

62 mineral, apatite. Building on Donelick et al., 2005 and Donelick and Chew, 2012,

63 Cogné et al., 2020 proposed a $\zeta-$based protocol, while other authors have suggested

64 using an absolute approach (e.g. De Grave et al., 2012; Soares et al., 2014,

65 Gleadow et al., 2015). Importantly, statistical methods for processing the LA-ICP-MS

66 data have been developed recently (Vermeesch, 2017, 2019) and we incorporate

67 these into the analysis we present later.

68   It has also been shown that laser spot ablation can also produce accurate U-

69 Pb and trace element data simultaneously during the analysis required for AFT data

70 (e.g. Chew and Donelick, 2012, Chew et al., 2016, Cogné et al., 2020). This is a big

71 advantage of the LA-ICP-MS method as the additional data can help to better

72 understand the AFT age data in both the analytical and geological contexts. In

73 contrast to the EDM method, application of the LA-ICP-MS approach can be

74 problematic in case of samples zoned in U. The EDM method produces an

75 approximate map of U concentration and typically both spontaneous and induced

76   tracks are counted on the same area, implicitly allowing for zoning to some degree.

77   For LA-ICP-MS only spontaneous tracks are counted and typically only a limited part

78   of the counted area is analyzed for U concentration by the ablation spot. Although

79   zonation in the z axis direction can be dealt with (Chew and Donelick, 2012, Cogné

80   et al., 2020), in-plane or horizontal zonation is less readily resolved by the routine

81   (i.e. single ablation spot) methods used in AFT dating. For samples with high

82   spontaneous track densities (ρ_s) the zonation is often visible in the spatial distribution

83   of spontaneous tracks. In that case, an analyst can select a counting area that is un-

84   zoned and/or close to the shape and size of the laser spot. However, dealing with

85   potential zoning becomes more problematic for samples with low ρ_s. If an analyst

86   selects a small area that mimics the laser spot then the number of counted tracks is

87   likely to be low and the uncertainty on a single grain age (SGA) increases. Two

88   methods have been proposed to overcome the zoning/low ρ_s issue, both requiring

89   counting tracks on a large area. Vermeesch (2017) suggested using multiple laser

90   spots (multi-spot) to improve understanding of the U distribution spatially. More

91   recently, Ansberque et al. (2020) proposed mapping the entire grain with a raster.

92   Both approaches, however, are time consuming and more expensive compared to

93   single spot analysis. Ideally, they then should be used only when necessary for

94   example if a large SGA dispersion is detected.

95   A second issue with the use of LA-ICP-MS is the commonly larger dispersion

96   of SGA compared to those from EDM. For example, Ketcham et al. (2018) reported

97   an interlaboratory experiment which consisted of blind dating two samples S1 and

98   S2. Of thirteen analysts, five used LA-ICP-MS and eight used EDM. The mean

99   dispersion for EDM was 2.5% for S1 and 2.1% for S2 while for LA-ICP-MS the mean

100 dispersion was 17.3% for S1 and 10.4% for S2. Regarding the canonical χ^2 test, that

101 is used to assess the possibility of single versus multiple or over-dispersed age

102 populations in a given sample, none of the EDM data sets failed the test ($p(\chi^2) <$

103 0.05) while three out of five of LA-ICP-MS dataset failed for S1 and two out of five for

104 S2. Such over-dispersion can be problematic because it could be used to infer

105 multiple age populations that do not really exist. In this context some authors have

106 suggested that the dispersion in SGA can be explained by the U content, or eU

107 content (eU = [U] + 0.235 [Th]) (e.g. Fernie et al., 2018; McDannell et al., 2019).

108 These authors demonstrated that the SGA from LA-ICP-MS are often older for lower

109 U grains and McDannell et al. (2019) argue for a radiation damage control on

110 annealing. Previously, Hendricks and Redfield (2005) proposed a similar α-radiation-

111 enhanced-annealing (REA) for EDM SGA data from the Fennoscandian shield.

112 However, Kohn et al. (2009) reconsidered the question using a different set of data

113 from various cratonic settings and concluded that there was no link between eU and

114 AFT age. This question is perhaps still open for the EDM, but has also become

115 topical for the LA-ICP-MS approach in the light of new datasets.

116 In this contribution we aim to test the multiple spot approach of Vermeesch

117 (2017) on samples of known age and also zoned and/or low ρ_s samples. We aim to

118 assess if this approach leads to decreased SGA dispersion in case of undetected

119 zonation. The second objective is to investigate if an inferred relationship between U

120 content and SGAs could be explained in part by such zonation.

121

122 <u>2- Samples and Methods</u>

123 *2.1 Samples*

124 We selected two apatite age standards: Fish Canyon Tuff (FCT – 28.1 ± 0.1

125 Ma, Boenhnke and Harrison, 2014) and Mount Dromedary (MtDrom – 98.5 ± 0.5 Ma,

126   McDougall and Wellman, 2011) because both are well characterized in terms of their

127   AFT ages, often being used as age standards. We selected eight additional samples,

128   all previously dated with AFT (EDM and/or LA-ICP-MS) from crystalline basement

129   from various tectonic settings (high and low exhumation rate) with known (because of

130   high track densities) or possible (unidentifiable because of low track densities) U

131   zoning, see Table 1 for details. Because all samples were previously dated, we can

132   test the accuracy of the multi-spot approach. The sample M1 was chosen because of

133   its visible zonation due to the high track density. However, this sample is treated as if

134   the zonation was not visible (i.e. spots for the multi-spot approach were randomly

135   positioned on the counted area). The motivation for doing this was to simulate what

136   could happen (increasing dispersion, SGA-U content correlation) when one has not

137   detected the zonation. The other samples were chosen because of the possible

138   zonation and / or low track density to assess how an unknown zonation can affect the

139   results of single versus multi-spot analysis.

140

141   *2.2 Methods*

142   All analyses were performed at the GeOHeLiS analytical platform (Univ.

143   Rennes, France) and follow the protocol of Cogné et al. (2020). All samples were

144   mounted in a 1.5 mm thick epoxy disc. The apatites were etched using a 5.5 M

145   HNO3 at 21°C for 20s. The grain mounting and etching are similar to the protocol

146   described by Donelick et al. (2005). Spontaneous fission track counting was carried

147   out using a Zeiss AxioImage M1 equipped with an automated stage system using

148   TrackWorks software at a magnification of 1000×. The U/Ca ratios, determined using

149   an ESI NWR193UC Excimer laser coupled to an Agilent 7700x Q-ICP-MS, were

150   used to calculate the ages (see Cogné et al., 2020 for details on the protocol). The

151   laser spot size was 30 μm with a repetition rate of 5 Hz and a fluence of 4 J/cm^2. All

152   instrumental conditions are summarized in the supplementary table S1.

153   For each grain the spontaneous track counting area was chosen to be large

154   enough to accommodate three to four ablation spots when possible. For the sample

155   M1 a smaller area was also delimited and counted to compare a "guided" single spot

156   approach with the multi-spot approach on the same grains. Guided here means that

157   the counted area is close in size and shape to the ablation spot and selected from a

158   region considered not too zoned, the low zonation being assessed on the basis of the

159   reasonably high and uniform track density (see Figure 1). For sample HIM 622/244

160   the whole grain area was counted irrespective of the size of the grain. We did this

161   because the track densities in this sample are so low that not taking into account the

162   whole area of the grains would tend to increase the estimated density and lead to

163   older SGA. The multi-spot approach of Vermeesch (2017) consists of calculating the

164   mean and variance U/Ca ratio from individual spots. We used IsoplotR (Vermeesch,

165   2018), in which the approach is implemented, to calculate central age, dispersion and

166    $p(\chi 2)$ for each sample. Pooled ages and associated uncertainties are calculated

167   using the spreadsheet discussed in Cogné et al. (2020) with single grain mean U/Ca

168   ratios and associated uncertainties calculated according to Vermeesch (2017).

169   Routinely, the U analysis for LA-ICP-MS FT dating is performed using only

170   one spot (e.g. Cogné et al., 2014, 2016). As previously explained, application of this

171   protocol to low ρ_s samples is problematic as it is not always obvious where to best

172   put the small ablation spot in the larger counted area. To simulate an effectively

173   random choice of ablation position, we used random sampling of multi-spot U/Ca

174   measurements to select one value for each grain and then calculate the equivalent

175   central age, dispersion and $p(\chi 2)$ of the sample. We repeated this sampling 2000

176   times, the goal being to compare what a standard single spot ablation approach

177   would have yield to the multi-spot approach in terms of accuracy and precision of the

178   central age and the dispersion of the SGA.

179

180   <u>3- Results</u>

181   The results are summarized in Table 2 and single grain data are provided as

182   supplementary data (Table S2). All multi-spot samples yielded similar pooled and

183   central ages and have $p(\chi^2)>0.05$. A large part of the samples actually exhibits high

184   p-value (>0.8) which might indicate an overestimation of the SGA uncertainty. The

185   low dispersion of SGA indicates a high probability of single age population, as it is

186   expected for bedrock sample. Guided single spot results for sample M1 also show

187    $p(\chi^2)>0.05$, although the dispersion of the SGA is larger than for multi-spot results

188   (Figure 1b and 1c). All ages are indistinguishable at the 2σ level of the published

189   ages except for HIM622/244 (Table 1, Figure 2). For that sample, the EDM reference

190   age is 0.03±0.04 Ma (Treloar et al., 2000), somewhat younger than the age in the

191   present study. However, our age is similar to that given by Ansberque et al. (2020)

192   also with LA-ICP-MS. We will discuss this difference in more detail below. The

193   relative central age uncertainties (presented as 2σ throughout the text) range from 5-

194   7% for 'normal' to high track density samples (MtDrom, FC1) to 25-33% for very low

195   track density samples (SG19, HIM 622/244), which is in the precision range of fission

196   track dating. The radial plots for the multi-spot data are shown on Figure 3, except for

197   sample M1 that is presented in detail on Figure 1. Single grain dots are color-coded

198   according to their mean U/Ca content.

199   To assess the degree of grain U/Ca zonation (Z) for a given sample we

200   calculate the relative uncertainty of the mean U/Ca ratio for each grain as calculated

8

201   by Vermeesch (2017), and then we take the average and standard deviation of that

202   ratio over all grains (equation 1).

203    $$Z = \frac{1}{N} \sum_{i=1}^{N} \left(\frac{\sigma_{U/Ca_i}}{\overline{U/Ca_i}} \right) \quad (1)$$

204   where N is the number of grains of the sample. If this average is low, then the intra

205   grain zonation is rather limited, even if the U concentrations in each grain may be

206   very different. Conversely if this value is high, this indicates a high proportion of

207   zoned grains in the sample.

208   In figure 4 we summarise the results from the 2000 random draws of one of

209   the multi-spot U/Ca ratios per grain.   For highly zoned samples (M1, SG9,

210   HIM622/244), most of the draws lead to a large SGA dispersion (averaging >40%),

211   involving failure of the χ^2 test 80-100% of the time. In contrast, samples with little

212   zoning (FCT, SG10, SG19, FC1) have low dispersion, rarely failing the χ^2 test (0-10%

213   of the time). Two moderately zoned samples (Pb1 and RM13) show intermediate

214   behaviour (χ^2 test 25-60% failure rate). An exception to this trend is the relatively

215   uniform MtDrom sample with draws that often (~60%) fail the χ^2 test. This case will be

216   further discussed below.

217   Figure 5 shows the radial plots for a single random draw for each sample,

218   except sample M1 that is already presented in detail on Figure 1. Single grain ages

219   are color-coded according to the U/Ca content. This figure shows that, even for less

220   zoned samples (e.g. FCT, SG10, SG19, FC1), the dispersion of random draw single

221   spot SGA increases relative to the multi-spot data. The increased dispersion will

222   potentially lead to failure of the χ^2 test. This dispersion is also associated with a

223   generally more pronounced apparent inverse correlation of the SGA with U content

9

224 (see supplementary material (Fig. S3) for plots of eU v age for the multi-spot and

225 single spot data).

226

227 <u>4- Discussion</u>

228 *4.1 Age accuracy and precision with multi-spot approach*

229   The central and pooled ages estimated using the multi-spot approach

230 reproduce the published literature ages well (Table 1 and Fig. 2), except the EDM

231 age of HIM622/244 (Treloar et al., 2000) which is discussed below. The precision of

232 SGAs using the multi-spot approach tends to be lower than when using a single spot

233 (see for example guided single spot vs multi-spot data for M1, Fig. 1b and 1c). This

234 effect seems to be larger for more highly zoned samples (compare Fig. 3 and 5),

235 such that the precision on SGA with multi-spot can half that when using a single spot.

236 For the single spot approach, the uncertainty on the U/Ca ratio comes directly from a

237 single ICP-MS measurement, while for the multi-spot approach it is calculated from

238 the different measurements of U/Ca on the same grain. Consequently, the more

239 zoned a sample is, the more variability of the individual U/Ca will increase, as will the

240 overall variance. Indeed, where the uncertainty (2σ) of single U/Ca measurement

241 was usually ca. 7% during this study, the uncertainty of mean U/Ca for a grain rises

242 to ca 60-70% for zoned samples or even 130% for HIM622/244. Therefore, while the

243 multi-spot approach gives a better understanding of the U/Ca distribution, the

244 resulting precision decreases strongly if the zonation is important. The decreasing

245 precision on the U/Ca ratio may induce an *under-dispersion* of the age data, leading

246 in turn to a relatively high p-value. This effect is potentially due to an over estimation

247 of U variability because we only use few measurements per grains (i.e. 2 to 4 spots).

248 In any case the under dispersion remains minor and we thus suggest that this does

249 not preclude the use of the multi-spot approach.

250   In a low ρ_s sample it is not possible to infer the zonation before ablation.

251 Therefore, reliably determining the central age of a sample using a single spot

252 approach would require using a counting area that mimics exactly the ablation spot.

253 For example, a sample with ρ_s ca. 1e5 tr/cm^2, a precision of U/Ca measurement of

254 7% and a precision of zeta of 1.5% (typical values in this study), 30 grains with a spot

255 of 30 μm diameter (typical number of counted grains and spot size) would result in a

256 central age uncertainty of ca. 45%. With a ρ_s of 1e4 tr/cm^2 the uncertainty rises to ca.

257 140%. Our samples with comparable ρ_s have central age uncertainties of ca. 15 to

258 25% using the multi-spot approach. To achieve similar precision with a single spot

259 approach, one would need to ablate ca. 100 to 1000 grains, for ρ_s of 1e5 and 1e4

260 tr/cm^2 respectively, which is time-consuming, and in turn could increase the risk of

261 over-dispersion by increasing the probability of using outliers grains.

262   It is thus preferable to use the multi-spot approach than the single spot

263 approach for low ρ_s samples. In addition to delivering a better understanding of U

264 distribution in each grain, it is more efficient in that we obtain a more reliable and

265 precise age. In high ρ_s samples, however, one might prefer to use a guided single

266 spot approach instead of using multi-spot as it is more precise, even with a lower

267 number of tracks counted, and faster, as demonstrated in the comparison for our M1

268 sample.

269   HIM622/244 is the only sample where we do not adequately reproduce the

270 EDM central age. However, our age is similar to that determined by Ansberque et al.

271 (2020), also obtained with LA-ICP-MS. These authors stated that the reasons for

272 discrepancy remain unclear. While we agree with that statement, we suggest two

273 possible reasons to partly explain the older ages obtained using LA-ICP-MS. Firstly,

274 the zero track grains represent half of the grains counted in this sample. The Cogné

275 et al. (2020) protocol, following Vermeesch (2017), does not attribute a zero Ma age

276 to zero spontaneous track grains, while this was most likely the case for Treloar et al.

277 (2000). If we assign a zero age to these zero track grains then the central age falls to

278 0.86 ± 0.76 Ma; closer, but still different, to the EDM age, and closer to our pooled

279 age of 0.45±0.21 Ma (Table 1). Secondly it is possible that we selected more grains

280 with tracks than Treloar et al. (2000), which can explain the older age we obtain or

281 equivalently Treloar et al, (2000) selected more zero track grains. The actual number

282 of zero track grains clearly impacts the final central or pooled ages. A random draw

283 of 20 grains from the 50 actually measured in this study, again repeated 2000 times,

284 and using a zero Ma age for the zero track grains reproduced the central age of

285 Treloar et al. (2000) ca. 13% of the time. Therefore, irrespective of this single

286 discrepant age, we reiterate that the central ages determined in this study using the

287 multi-spot approach agree well with the vast majority of published ages.

288

289 *4.2 The effects of U zonation on LA-ICP-MS FT dating*

290 In the examples of our random draws (Fig. 5), we see that high-U grains (red

291 colours on Fig. 5) tend to have younger ages while the older ages are from low-U

292 grains (yellow colours). Some correlation of U and SGA is expected based on

293 statistical arguments (Pearson, 1896). The fission track age equation can be

294 approximated to a good precision by a linear equation in which the age (t) is

295 proportional to the ratio of ρs to U concentration following (eq.5 of Vermeesch, 2017):

296 $$t = \frac{1}{\lambda_d} ln\left(1 + \frac{\lambda_d}{\lambda_f} \frac{2N_s}{[^{238}U]A_sLq}\right) \approx \frac{2\rho_s}{\lambda_f[^{238}U]Lq} \propto \frac{\rho_s}{[^{238}U]} \quad (2)$$

297 Given this we expect t to be negatively correlated with [U] to some extent (we can

298 imagine plotting $\frac{\rho_s}{[U]}$ v [U]). Thus, even on multi-spot data a correlation may exist but

299 it is clearly more important when looking at the single spot data (Fig. S3), and it

300 becomes visible on radial plots.

301   Moreover, when using single U/Ca measurement the dispersion increases,

302 and p(χ^2) decreases, compared to the multi-spot results (Fig. 4). Therefore, an

303 inverse correlation between U/Ca content and SGA appears along with over-

304 dispersion. This is illustrated at the scale of a grain in Figure 6a. This radial plot

305 shows SGA for one grain of sample M1. The multi-spot age includes the total number

306 of tracks counted on the larger blue area illustrated on Fig. 1a. As the number of

307 spontaneous tracks appropriately reflects the mean U/Ca measured on the 3 spots,

308 the resultant multi-spot single grain age is in line with the central age of the sample.

309 The "guided" single count is similar to the multi-spot age, but more precise as

310 explained above. Finally spot 1, spot 2 and spot 3 ages use the large area for the

311 spontaneous track count and only one U/Ca measurement. The calculated ages are

312 more precise but more dispersed compare to the central age as the single U/Ca

313 measured is not representative of the whole counted area. Several similarly

314 unrepresentative measurements would lead to over-dispersion. Furthermore, the

315 ages are inversely related to the U content. To summarise, both the over-dispersion

316 and inverse correlation are attributable in this example to single spot U/Ca

317 measurements not being representative of the mean in the region where the

318 spontaneous tracks were counted for the given grain.

319   At the scale of the whole M1 sample we also plotted all the possible SGAs

320 depending on which spot is used (i.e. 1 to 4 ages per grain, using the same count

321 and area but the different U/Ca measurements, Fig. 6b). This clearly highlights the

13

322 tendency for higher U/Ca to be associated with younger and generally more precise

323 ages (the bottom right part of the radial plot). When considering the ensemble of

324 single spots on figure 6b an apparent inverse correlation between U content and age

325 is obvious. However this is an artefact of the spot position, as the multi-spot and

326 "guided" single spot data (figure 1 b,c) do not show this behaviour. While the

327 zonation is visible on this sample, the same effect would appear on sample on which

328 the zonation would have remained undetected.

329 Random draw data for Mt Dromedary or FC1 show that, even on relatively un-

330 zoned and 'normal' track density samples, misplacing a spot on only few slightly

331 zoned grains can results in an over-dispersion from time to time. On MtDrom

332 especially, about 60% of our random draws failed the χ^2 test despite a low degree of

333 U zoning. As increasing precision of single grain ages increases the possibility of

334 inferring over-dispersion statistically, this is likely due to the relatively high track

335 densities in this sample. As detailed above, over-dispersion of SGA in a sample can

336 also arise from an unrepresentative determination of the U content of the counted

337 area. Thus, with a larger number of tracks the SGA becomes more precise and

338 smaller variations of U/Ca can increase the dispersion.

339 Therefore, over-dispersion of SGA can be the result of older or younger ages

340 relative to the true age. However, as summarised in Table 2, sample central ages

341 calculated from random draws for single spots are undistinguishable from the central

342 ages determined using the multi-spot data at the 2σ level (except for 5 draws out of

343 2000 on M1 sample). Even at the 1σ level the vast majority of the central ages

344 (almost 100% of the random draws for most samples, and >90% for the others) are

345 undistinguishable from the multi-spot central ages. This is likely the result of

346 compensation between too old grains and too young grains for the single spot data.

347 This result, based on the experiments presented here, suggests that although the

348 dispersion increases slightly the uncertainty on the single spot central age, it has

349 minimal impact on its accuracy. In case of extreme core rim zonation, the problem

350 could be enhanced but such configuration is probably rare. This is particularly

351 important, because it implies that LA-ICP-MS ages for basement samples that show

352 a high degree of dispersion likely remain accurate, the dispersion potentially coming

353 from undetected zoning and / or spot misplacement during laser ablation.

354 However, the U-SGA relationship reported in some publications (e.g. Fernie et

355 al., 2018, McDannell et al., 2019) could still reflect other controls. As the factors that

356 determine track annealing kinetics are crucial to understand and interpret FT data, it

357 is clearly of primary importance to know if U content is an influential factor or not. In

358 assessing this, we suggest here that when a relationship between U content and

359 SGA is apparent in data collected using one ablation spot per grain, a second LA-

360 ICP-MS session should be performed to see if this is really linked to U content or

361 may due to initially undetected zoning.

362

363 *4.3 Recommendations when dealing with low ρ_s samples*

364 When the spontaneous track density is too low to visualise possible zonation,

365 three different approaches are possible, (i) counting an area that exactly mimics the

366 ablation spot, (ii) using the mapping approach of Ansberque et al. (2020) and (iii)

367 using the multi-spot approach of Vermeesch et al. (2017). The first solution is the

368 fastest but is not precise as it limits the size of the counting area and consequently

369 reduces the number of countable tracks. The two other approaches are more time

370 consuming, limiting output to roughly two basement samples for a day of ICP-MS

371 analysis. Comparing the samples that were presented in both Ansberque et al.

372   (2020) and our study (RM 13, HIM622/244 and FCT), it appears that the mapping

373   approach yields more precise SGA data, and so a more precise central age. This is

374   mostly due to the U/Ca measurement protocol and counting statistics. The mapping

375   approach relies on averaging U/Ca for all pixels of the grain map. Given a pixel is

376   about 3.5 μm wide, one ends up with a few hundred pixels for a grain and thus a few

377   hundred U/Ca ratios. With the multi-spot approach, we typically use 3 to 4 spots per

378   grain. It is obvious that the standard error of the mean U/Ca concentration will be

379   larger with four counts than with a few hundred and so leads to a less precise age

380   estimate. However, the mapping approach necessitates equipment and materials

381   that are not currently available in all LA-ICP-MS laboratories. Additionally, once one

382   has decided to use the mapping approach, it has to be done for the whole sample

383   and this choice implies half a day of ICP-MS time. In contrast the multi-spot approach

384   is more practical and flexible for basement samples as one could decide to do only

385   one spot during a first session. If the single grain dispersion is low then there is no

386   obvious need to perform more analysis. Alternatively, if the dispersion is high, one

387   should do more spots, at least on the grains that are responsible for the over-

388   dispersion, to assess if the dispersion reflects a zoning issue or could be a sign of

389   differential annealing behaviour. For detrital samples, the preferred procedure is

390   harder to define as we may anticipate multiple age populations and different

391   annealing effects, typically requiring analysis of a large number of grains (c. 120

392   grains per sample) to characterise adequately the distribution of SGA. Using the

393   multi-spot approach on for each grain would be time consuming but in detrital

394   samples, one cannot generally rely on the SGA dispersion to indicate analytical

395   issues. In such cases it is possible to try and initially characterise different

396   populations using other data acquired simultaneously, such as U-Pb ages or trace

397 element concentrations (e.g. O'Sullivan et al., 2020, Westerweel et al., 2020). Then,

398 at least in principle, different populations or components can be isolated and the

399 analyst can decide if more spots are needed on some grains.

400

401 5- Conclusion

402   In this study we assessed the multi-spot approach proposed by Vermeesch

403 (2017) in terms of its ability to decrease SGA dispersion in low ρ_s and / or zoned

404 samples. It also increases the precision on the central age by allowing the counting

405 larger areas. Our results show that this method is efficient and should be used when

406 SGA over-dispersion is apparent for a basement sample. Moreover, we show that an

407 inverse correlation between SGA and U content coupled to over dispersion can be

408 induced due to zoning and single spot U contents being unrepresentative of the

409 whole grain. This means that U zoning could give a potentially false impression that

410 high/low U content leads to faster/slower annealing. Therefore, it is important to

411 assess if multi-spot datasets continue to give such relationships in slowly cooled

412 basement samples to better understand and better interpret FT data.

413

414 6- Acknowledgements

422

423   7- References

424   Ansberque, C., Chew, D.M., Drost, K. 2021, Apatite fission-track dating by LA-Q-ICP-
425   MS mapping. Chemical Geology, 560, 119977.

426   Boehnke, P., Harrison, M.T., 2014. A meta-analysis of geochronologically relevant
427   half-lives: what's the best decay constant? International Geology Review, 56,
428   905-914.

429   Brichau, S., Ring, U., Carter, A., Bolhar, R., Monié, P., Stockli, D., Brunel, M., 2008.
430   Timing, slip rate, displacement and cooling history of the Mykonos detachment
431   footwall, Cyclades, Greece, and implications for the opening of the Agean Sea
432   basin. Journal of the Geological Society 165, 263-277.

433   Chew, D.M., Donelick, R.A., 2012. Combined apatite fission track and U-Pb dating by
434   LA-ICP-MS and its application in apatite provenance analysis. Mineralogical
435   Association of Canada Short Course 42, 219-247.

436   Chew, D.M., Babechuk, M.G., Cogné, N., Mark, C., O'Sullivan, G.J., Henrichs, I.A.,
437   Doepke, D., McKenna, C.A., 2016. (LA,Q)-ICPMS trace-element analyses of
438   Durango and McClure Mountain apatite and implications for making natural LA-
439   ICPMS mineral standards. Chemical Geology, 435, 35-48.

440   Cogné, N., Chew, D.M., Stuart, F.M., 2014. The thermal history of the western Irish
441   onshore. Journal of the Geological Society, 171, 779-792.

442   Cogné, N., Doepke, D., Chew, D.M., Stuart, F.M., Mark, C., 2016. Measuring plume-
443   related exhumation of the British Isles in Early Cenozoic times. Earth and
444   Planetary Science Letters 456, 1-15.

445 Cogné N., Chew., D.M., Donelick, R.A., Ansberque, C., 2020. LA-ICP-MS apatite

446   fission track dating: a practical zeta-based approach. Chemical Geology 531,

447   119302

448 De Grave, J., Glorie, S., Ryabinin, A., Zhimulev, F., Buslov, M.M., Izmer, A., Elburg,

449   M., Vanhaecke, F., Van den haute,P., 2012. Late Palaeozoic and Meso-

450   Cenozoic tectonic evolution of the southern Kyrgyz Tien Shan: Constraints from

451   multi-method thermochronology in the Trans-Alai, Turkestan-Alai segment and

452   the southeastern Ferghana Basin. Journal of Asian Earth Sciences, 44, 149-168.

453 Donelick, R.A., O'Sullivan, P.B., Ketcham, R.A., 2005. Apatite Fission-Track

454   Analysis. Reviews in Mineralogy and Geochemistry 58, 49-94.

455 Fernie, N., Glorie, S., Jessel, M.W., Collins, Collins, A.S., 2018. Thermochronological

456   insights into reactivation of a continental shear zone in response to Equatorial

457   Atlantic rifting (northern Ghana). Scientific Reports 8, 16619.

458 Gleadow, A., Harrison, M., Kohn, B., Lugo-Zazueta, R., Phillips, D., 2015. The Fish

459   Canyon Tuff: a new look at an old low-temperature thermochronology standard.

460   Earth and Planetary Science Letters 424, 95-108.

461 Hasebe, N., Barbarand, J., Jarvis, K., Carter, A., Hurford, A.J., 2004. Apatite fission-

462   track chronometry using laser ablation ICP-MS. Chemical Geology 207, 135-145.

463 Hendriks B. and Redfield T. (2005) Apatite fission track and (U- Th)/He data from

464   Fennoscandia: an example of underestimation of fission track annealing in

465   apatite. Earth and Planetary Science Letters 236, 443–458.

466 Henrichs, I.A., O'Sullivan, G.J., Chew, D.M., Mark, C., Babechuk, M.G., McKenna,

467   C., Emo R., 2018. The trace element and U-Pb systematics of metamorphic

468   apatite. Chemical Geology, 483, 218-238.

469   Hurford, A.J., 1990. Standardization of fission track dating calibration:

470   Recommendation by the Fission Track Working Group of the I.U.G.S.

471   Subcommission on Geochronology. Chemical Geology 80, 171-178.

472   Hurford, A.J., Green, P.F., 1983. The zeta age calibration of fission-track dating.

473   Chemical Geology 41, 285-317.

474   Iwano, H., Danhara, T., Yuguchi, T., Hirata, T., & Ogasawara, M., 2019. Duluth

475   complex apatites: Age reference material for LA–ICP–MS– based fission–track

476   dating. Terra Nova, 31, 247–256.

477   Jolivet, M., Roger, F., Xu, Z.Q., Paquette, J-L, Cao, H., 2015. Mesozoic-Cenozoic

478   evolution of the Danba dome (Songpan Garzê, East Tibet) as inferred from LA-

479   ICPMS U-Pb and fission-track data. Journal of Asian Earth Sciences 102, 180-

480   204.

481   Ketcham, R.A., van der Beek, P., Barbarand, J., Bernet, M., Gautheron, C., 2018.

482   Reproducibility of thermal history reconstruction from apatite fission-track and (U-

483   Th)/He data. Geochemistry, Geophysics, Geosystems, 19, 2411-2436.

484   Kohn B. P., Lorencak M., Gleadow A. J., Kohlmann F., Raza A., Osadetz K. G.,

485   Sorjonen-Ward P., 2009. A reappraisal of low-temperature thermochronology of

486   the eastern Fennoscandia Shield and radiation-enhanced apatite fission-track

487   annealing. In: Lisker, F., Ventura, B., Glasmacher, U.A. (Eds.).

488   Thermochronological methods: from paleotemperature constraints to landscape

489   evolution models. Geological Society of London Special Publication 324, 193–

490   216.

491   McDannell, K.T., Issler, D.R., O'Sullivan, P.B., 2019, Geochimica et Cosmochimica

492   Acta, Radiation-enhanced fission track annealing revisited and consequences for

493   apatite thermochronometry, 252, 213-239.

494 McDougall, I., Wellman, P., 2011. Calibration of GA1550 biotite standard for K/Ar and

495 $^{40}Ar/^{39}Ar$ dating. Chemical Geology, 280, 19-25.

496 O'Sullivan, G.O., Chew, D., Kenny, G., Henrichs, I., Mulligan, D., 2020. The trace

497 element composition of apatite and its application to detrital provenance studies.

498 Earth-Science Reviews, 201, 103044.

499 Paton, C., Hellstrom, J., Paul, B., Woodhead, J., Hergt, J., 2011. Iolite: Freeware for

500 the visualisation and processing of mass spectrometric data. Journal of Analytical

501 Atomic Spectrometry 26, 2508-2518.

502 Pearson, K. 1896. Mathematical contributions to the theory of evolution.-On a form of

503 spurious correlation which may arise when indices are used in the measurement

504 of organs. Proceedings of the Royal Society of London, 60, 489–498.

505 Price, P., Walker, R., 1962. Observation of Fossil Particle Tracks in Natural Micas.

506 Nature 196, 732–734.

507 Soares, C., Guedes, S., Hadler, J., Mertz-Kraus, R., Zack, T., Iunes, P., 2014. Novel

508 calibration for LA-ICP-MS-based fission-track thermochronology. Physics and

509 Chemistry of Minerals 41, 65-73.

510 Treloar, P.J., Rex, D.C., Guise, P.G., Wheeler, J., Hurford, A.J., Carter, A., 2000.

511 Geochronological constraints on the evolution of the Nanga Parbat syntaxis,

512 Pakistan Himalaya. In: Khan, M.A., Treloar, P.J., Searle, M.P., Jan, M.Q. (Eds).

513 Tectonics of the Nanga Parbat Syntaxis and the Western Himalaya. Geological

514 Society of London Special Publication 170, 137-162.

515 Vermeesch, P., 2017, Statistics for LA-ICP-MS based fission track dating. Chemical

516 Geology, 456, 19-27.

517 Vermeesch, P., 2018. IsoplotR : A free and open toolbox for geochronology.

518 Geosciences Frontiers, 5, 1479-1493.

519 Vermeesch, P., 2019. Statistics for fission-track thermochronology, in: Fission-track

520   thermochronology and its application to geology, M. Malusà and P. Fitzgerald

521   Eds., Springer, Berlin. 393pp.

522 Westerweel, J., Licht, A., Cogné, N., Roperch, P., Dupont-Nivet, G., Kay Thi, M.,

523   Swe, H. H., Huang, H., Win, Z., Aung, D.W., 2020. Burma Terrane collision and

524   northward indentation in the Eastern Himalayas recorded in the Eocene-Miocene

525   Chindwin Basin (Myanmar). Tectonics, 39, e2020TC006413.

526 Woodhead, J., Hellstrom, J., Hergt, J., Greig, A. and Maas, R., 2007. Isotopic and

527   elemental imaging of geological materials by laser ablation Inductively Coupled

528   Plasma mass spectrometry. Journal of Geostandards and Geoanalytical

529   Research 31, 331-343.

530

531 <u>Figure caption</u>

532 Table 1: Samples used in this study.

533

534 Table 2: Results for fission track analysis and random draws. Detailed grain data are

535 provided in supplementary material.

536

537 Figure 1: Example of grain area determination and data for M1 sample (a) Example

538 of how we used two different spontaneous track counting areas, the emplacement of

539 the three ablation spots and the counted tracks. (b) Radial plots for the multi-spot

540 data. (c) Radial plots of the "guided" single spot data (counted area close in size and

541 shape to the ablation spot and from a region relatively unzoned). (d) Radial plots of

542 one random draw. The data are over-dispersed and SGA seems related to the U/Ca

543 content. See text for further discussion.

544

545

546   Figure 2: Plot of the central ages calculated in this study versus literature central

547   ages for all samples. Note the logarithmic scale for both axis and the break on the y-

548   axis. The dashed line is the 1:1 line

549

550   Figure 3: Radial plots for all samples using multi-spot data. All samples yield ages in

551   agreement with the published values and show a low degree of dispersion. CA =

552   Central age

553

554   Figure 4: (a) The proportion of random draws that pass the $\chi 2$ test (p($\chi 2$)>0.05)

555   versus the U/Ca variation in the sample, showing a negative correlation.. (b) Mean

556   dispersion of the 2000 random draws versus the U/Ca variation in the sample,

557   showing a positive correlation..

558

559   Figure 5: An example of the random sampling to simulate single spot data for the

560   different samples. For all samples the SGA dispersion increases compared to the

561   multi-spot data (Fig. 3). In some samples the SGA seem correlated to U/Ca content

562   (color-coded for each grain) - younger and often more precise ages with higher U/Ca.

563   However, all central ages are undistinguishable from those estimated with the multi-

564   spot data. CA = Central age

565

566   Figure 6: (a) Radial plot of a single grain age from M1 grain 30 data calculated using

567   multi-spot, "guided" single count (tracks counted in the white area in Fig. 1a), and

568   spot 1, spot 2, spot 3, that use tracks counted in the blue area in Fig. 1a and the

569   measured U/Ca ratio from spot 1, 2 or 3 respectively. Spot 1 samples more or less

570   the average U/Ca ratio. We see that when the ablation spot hits a higher than

571   average U area, the age is younger (spot 3) while when it hits a lower U area the age

572   is older (spot 2). (b) Radial plots of all the possible SGA, implying an apparent

573   inverse relation between U/Ca content and SGA. See text for further discussion.

574

575

Sample Name and Location	lithology	Reported age	Characteristics	Reference
Fish Canyon tuff (USA)	Tuff	28.1 ± 0.1	Age standard	Boenhnke and Harrison, 2014
Mt Dromedary (NSW, Australia)	Granite	98.5 ± 0.5	Age standard	McDougall and Wellman, 2011
FC1 (Duluth Complex, USA)	Anorthositic serie	861 ± 29 °*	proposed reference material; low exhumation rate	Iwano et al., 2019
M1 (Mykonos, Greece)	Monzogranite	12.5 ± 2.2*	High track density; visible zonation; high exhumation rate	Brichau et al., 2008
RM13 (Paros, Greece)	Paragneiss	9.9±0.6°	low track density; known zonation; high exhumation rate	Henrichs et al., 2018; Ansberque et al., 2020
Pb1 (Wales)	Granite	220.8 ± 52.0°	low track density; possible zonation; low exhumation rate	Cogné et al., 2016
HIM 622/244 (Nanga Parbat Massif, Pakistan)	Gneiss	0.03 ± 0.04*; 0.8 ± 0.3°	very low track density; possible zonation, high exhumation rate	Treloar et al., 2000; Ansberque et al., 2020
SG9 (Danba Dome, Eastern Tibet)	Gneiss	5.7 ± 0.7*	low track density; possible zonation, high exhumation rate	Jolivet et al., 2015
SG10 (Danba Dome, Eastern Tibet)	Leucocratic dyke	4.5 ± 0.6*	low track density; possible zonation, high exhumation rate	Jolivet et al., 2015
SG19 (Danba Dome, Eastern Tibet)	Granite	4.7 ± 0.7*	low track density; possible zonation, high exhumation rate	Jolivet et al., 2015

° Reference Age determined with LA-ICP-MS

* Reference Age determined withEDM

	nb grains	Ns	Area (cm2)	ρs (track/cm2)	U/Ca	p(χ2)	Dispersion (%)	central age±2σ (Ma)	pooled age±2σ (Ma)	reference age±2σ (Ma)	Uranium variation (a)	Random Ages (%) (b)	Random p(χ2) (%) (c)	Random dispersion (d)
M1 (Single spot)	30	754	6.33E-04	1.19E+06	1.03E-01	0.06	13.2	10.3 ± 0.9	10.0 ± 0.8	12.5 ± 2.2*	-			
M1 (Multi spots)	30	1642	1.63E-03	1.00E+06	7.25E-02	1	0	10.0 ± 1.5	9.6 ± 1.8	12.5 ± 2.2*	0.37 ± 0.05	99.9 / 92.9	0	0.53 [0.36-0.66]
RM13	40	244	2.29E-03	1.06E+05	6.94E-03	0.87	0	11.2 ± 1.7	10.3 ± 1.6	9.9±0.6°	0.22 ± 0.02	100 / 99.9	37.1	0.26 [0.00-0.44]
SG9	30	145	1.40E-03	1.03E+05	1.50E-02	0.97	0	5.0 ± 1.1	4.7 ± 1.0	5.7 ± 0.7*	0.31 ± 0.06	100 / 98.5	19.9	0.44 [0.00-0.74]
SG10	29	70	1.79E-03	3.91E+04	6.45E-03	0.93	0	5.2 ± 1.3	4.4 ± 1.1	4.5 ± 0.6*	0.14 ± 0.02	100 / 100	100	0.00 [0.00-0.12]
SG19	30	62	1.82E-03	3.40E+04	4.75E-03	1	0	5.5 ± 1.4	4.9 ± 1.3	4.7 ± 0.7*	0.12 ± 0.02	100 / 100	100	0.00 [0.00-0.00]
Pb1	28	228	9.95E-04	2.29E+05	7.33E-04	0.94	0	214.8 ± 34.0	203.3 ± 34.6	220.8 ± 52.0°	0.19 ± 0.06	100 / 99.6	74.8	0.19 [0.00-0.52]
FC1	20	1862	7.60E-04	2.45E+06	1.83E-03	0.92	0	882.4 ± 44.4	879.7 ± 46.6	861 ± 29 °*	0.04 ± 0.01	100 / 99.8	91.2	0.04 [0.00-0.11]
HIM622/244	50	30	8.21E-03	3.65E+03	5.56E-03	0.2	37.5	1.2 ± 0.5	0.45 ± 0.21	0.03 ± 0.04*; 0.8 ± 0.3°	0.64 ± 0.04	100 / 100	0	0.62 [0.55-0.74]
Fish Canyon Tuff	28	236	1.23E-03	1.92E+05	4.81E-03	0.84	0	29.0 ± 4.0	27.7 ± 3.8	28.1 ± 0.1	0.09 ± 0.01	100 / 100	100	0.01 [0.00-0.14]
MtDromedary	20	945	7.38E-04	1.28E+06	9.13E-03	0.63	0	96.5 ± 7.0	95.8 ± 7.1	98.5 ± 0.5	0.06 ± 0.01	100 / 99.5	40.9	0.11 [0.00-0.19]

° Reference Age determined with LA-ICP-MS

* Reference Age determined withEDM

(a) Defined as the average ± standard deviation of the relative standard deviation of U/Ca ratio of each grain

(b) Percentage of random draw that yielded the same central age than multiple spots within 2σ /within 1σ

(c) Percentage of random draw that have p(χ2) >0.05

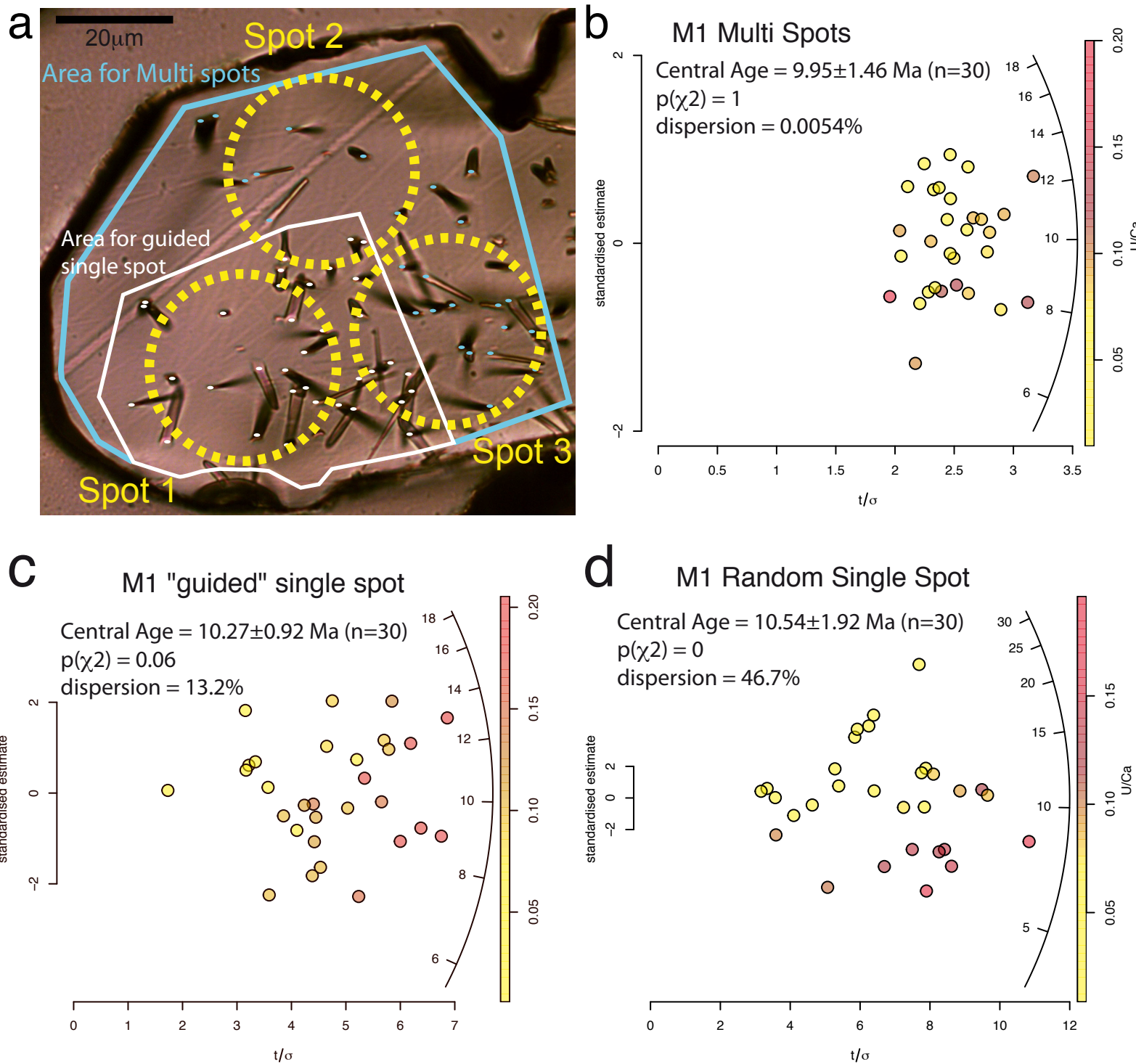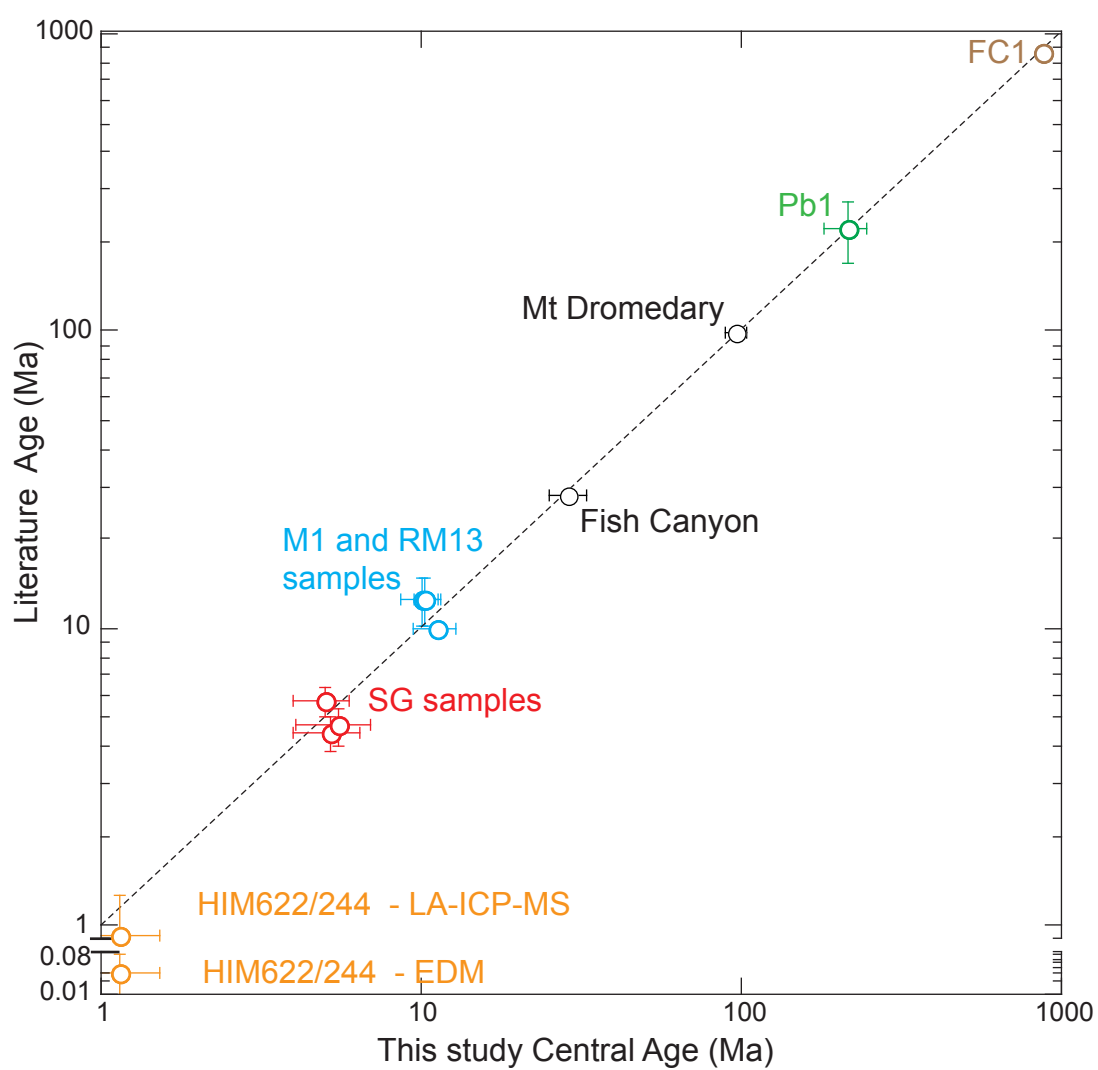(d) Average and 95% asymetric interval of dispersion of single grain age of random draw
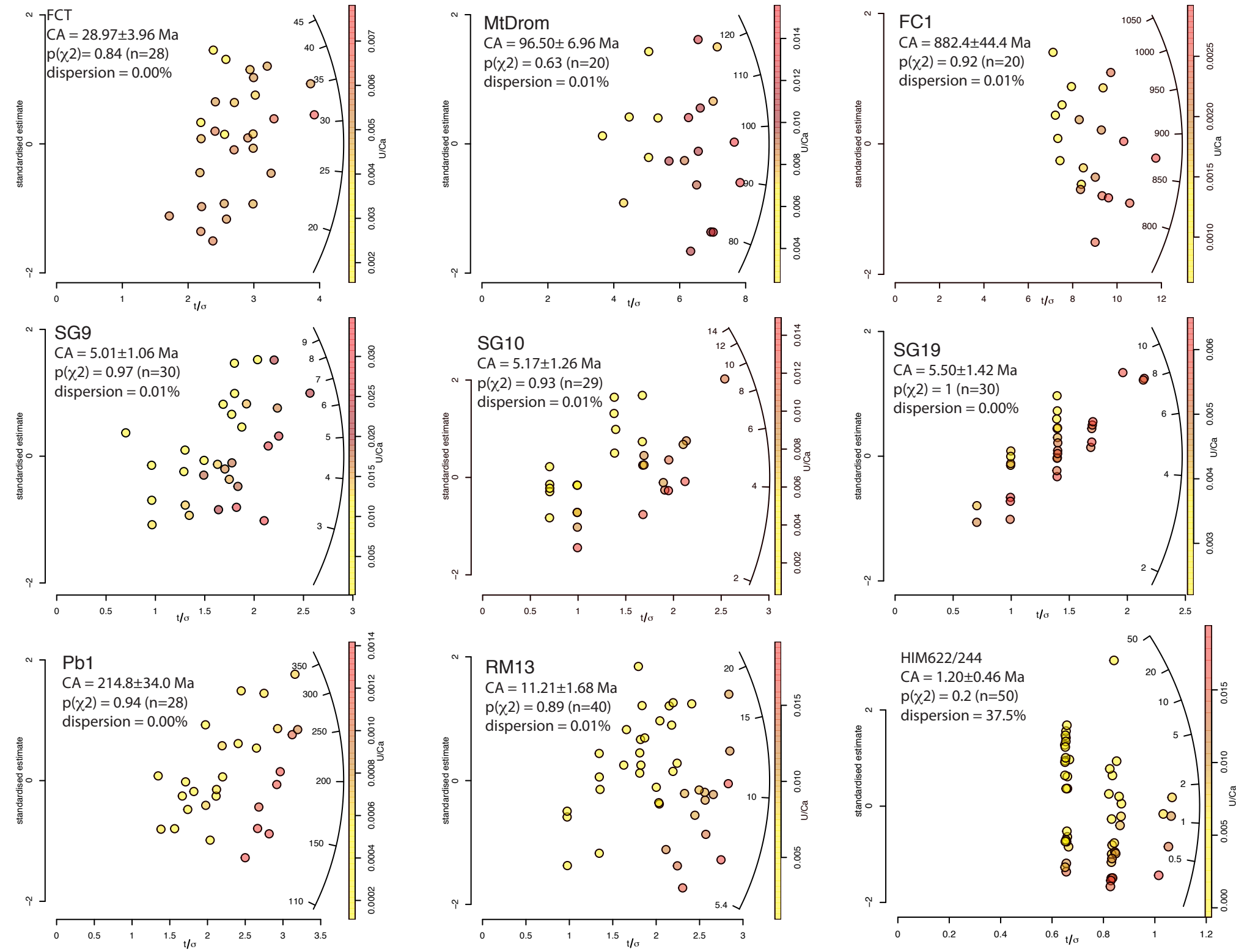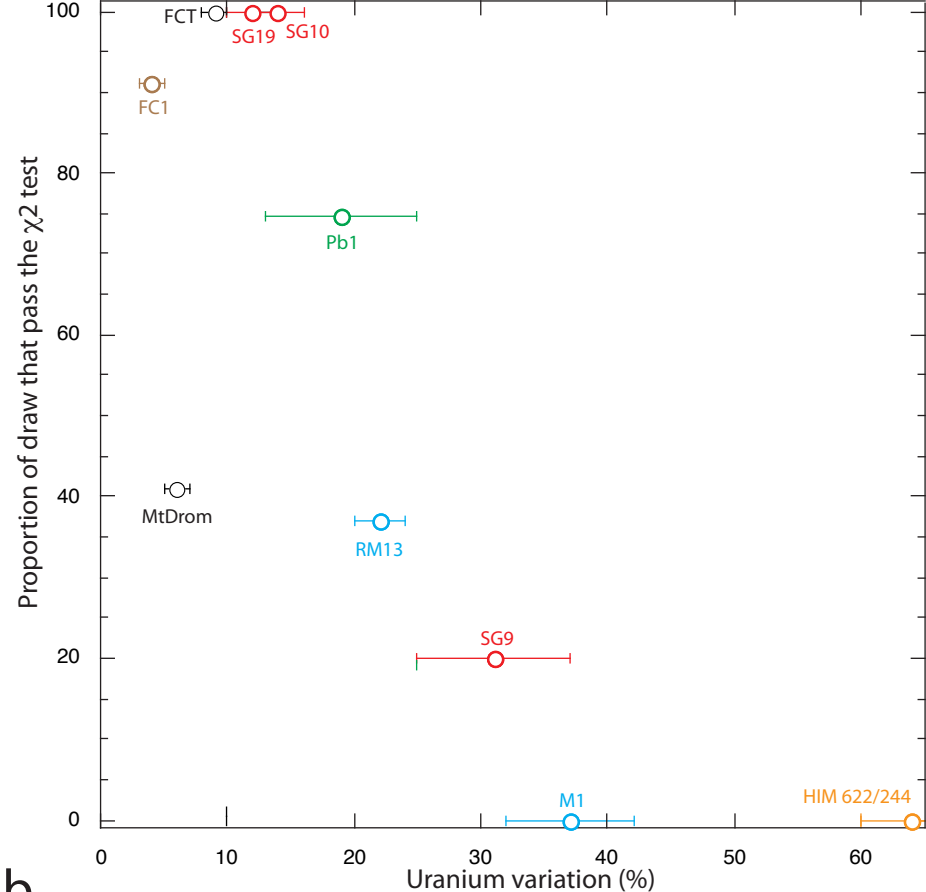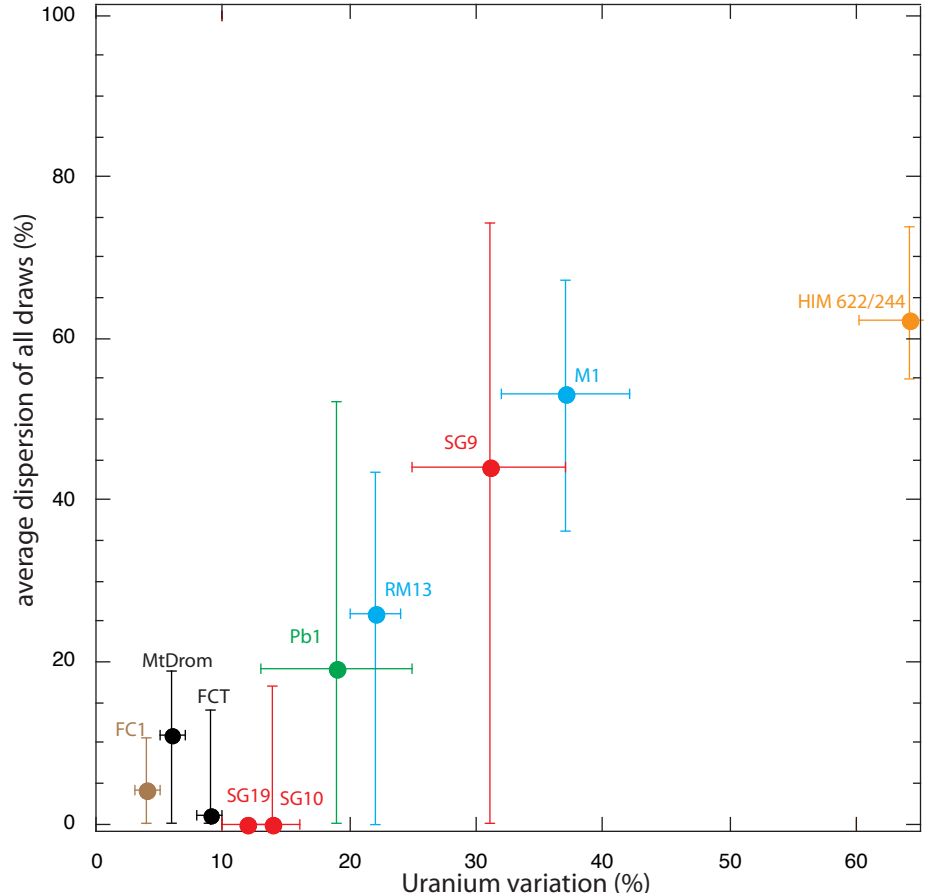
Figure 1

Figure 2

Figure 3

Figure 4

Figure 5

Figure 6

a

M1 - grain 30

Spot 2
20
18
16
14
12
"Guided"
single count
10
Spot 1
Multi Spots
8
Spot 3

standardised estimate

U/Ca
0.12
0.10
0.08
0.06

t/σ

b

M1 - All age data

Central Age = 9.98±1.18 Ma (n=95)
p(χ2) = 0
dispersion = 55.3%

47
20
10
5
3
2

standardised estimate

U/Ca
0.20
0.15
0.10
0.05

t/σ